J. Fluid Mech. (1999), *vol.* 381, *pp.* 199–223. Printed in the United Kingdom

Cyclone and anticyclone formation in a rotating stratified fluid over a sloping bottom

By C. CENEDESE† AND P. F. LINDEN

Department of Applied Mathematics and Theoretical Physics, The University of Cambridge, Silver Street, Cambridge CB3 9EW, UK

(Received 30 January 1998 and in revised form 16 September 1998)

We discuss laboratory experiments with a continuous source or sink of fluid in a two-layer rotating environment which produces anticyclonic and cyclonic vortices, respectively. Experiments were carried out with a sloping bottom in order to simulate the β-effect and they were conducted for different values for the source/sink flow rate Q and the Coriolis parameter f. The Rossby number Ro of these vortices was small but finite and the flow was expected to be quasi-geostrophic. The qualitative behaviour of the anticyclonic and cyclonic vortices was generally similar, but it depended on the flow rate. For low flow rates, a single vortex formed at the source and extended to the west. At higher flow rates, the vortex broke free from the source and moved to the west; this vortex was then followed sequentially by other vortices behaving similarly. The westward velocity U of these vortices was calculated and compared with the speed U_s of a linear topographic Rossby wave. For multiple vortices the westward velocities were greater than U_s while for a single vortex produced by a low flow rate the velocity was less than U_s. Significant asymmetry between the anticyclonic and cyclonic vortices was observed in the transition zone from single to multiple vortices which implies that ageostrophic effects were still present in the flow.

1. Introduction

In the last 20 years, several surveys in the Canary Basin of the eastern Atlantic have shown the presence of Mediterranean water in lens-shaped vortices called 'Meddies'. These lenses are all double convex and rotate anticyclonically (Armi & Zenk 1984; Pingree & Le Cann 1993). The continuous Mediterranean outflow through the Strait of Gibraltar develops into a coastal current along the coast of Spain and Portugal and provides the water found within the Meddies (Bower, Armi & Ambar 1996). These eddies play an important role in maintaining the temperature and salinity distributions in the North Atlantic, but relatively little is known about their early life histories, including where and how often they form, and the mechanism by which the continuous Mediterranean outflow breaks into discrete coherent vortices. In this paper we report laboratory experiments which elucidate how a continuous source (or sink) with a constant flow rate of fluid can generate discrete vortices. The results should also be of relevance to the behaviour of surface eddies formed from a surface coastal current of buoyant water over a continental slope.

Meddies are characterized by their high salinity and temperature relative to the surrounding water and have a radius of approximately 50 km, a vertical extent of about 1 km and a core depth in the range 1100–1200 m. The azimuthal velocity

† Present address: WHOI, 360 Woods Hole Rd, Woods Hole, MA 02543, USA; e-mail ccenedese@whoi.edu.

of these lenses is approximately 0.2 m s^{-1} at radii between 30 and 45 km. After their formation, Meddies are advected rapidly along the topography with a velocity ranging between 13 cm s^{-1} and 34 cm s^{-1} (Bower *et al.* 1996). They are observed to be long-lived structures (Armi *et al.* 1988) with a translation that is mainly to the South covering 1100 km in two years. Two dimensionless parameters are important for this kind of flow: the Rossby number $Ro = \zeta/f$, where ζ is the relative vorticity and f is the planetary vorticity, and the Burger number $B = (g'H)^{1/2}/fL$, where g' is the reduced gravity, H is the fluid depth and L is a characteristic horizontal lengthscale. For Meddies $Ro \approx 0.04$ and $B \approx 2$. A low Rossby number suggests that the flow is quasi-geostrophic and a Burger number of order of unity suggests that the buoyancy forces and the Coriolis forces are in balance, since the horizontal scale of the motion is of the same order of magnitude as the Rossby radius of deformation.

Davey & Killworth (1989) determined the flow produced by a confined source of buoyancy in an otherwise single layer of water using a reduced-gravity model on a β-plane (the upper layer is assumed to be passive). In their numerical model the source filled an area of the order of the Rossby deformation radius across and the flow rate was constant. A nonlinear shallow-water model was used and the solution gave three regimes. For weak forcing the solution was linear and a single vortex was produced, taking the form of a 'tube' of fluid extending westward from the source as a zonal flow, with north–south flow only near the source and at the front of the extending tube. With increasing amplitude of the forcing nonlinear terms became significant. The zonal flow was then unstable and a series of anticyclonic eddies, each of which propagated westward, was observed. For greater forcing the motion was not resolved by their numerical calculation.

Laboratory experiments investigating the flow produced by a source of less-dense fluid in an otherwise single-layer rotating environment were conducted by Linden (1991). A sloping bottom was used in order to simulate the β-effect. Anticyclonic vortices developed at the surface and two different patterns of behaviour were observed. At low flow rates a single vortex formed in the centre of the tank and extended to the west. For larger flow rates a single vortex broke free from the source and moved to the west, followed by other vortices behaving in the same fashion. In these experiments the vortex was isolated inside the denser layer and the interface beneath the vortex surfaces intersected the free surface to form a front.

The present paper is an extension of this work in two respects, both associated with the effects of finite Rossby number. The introduction of buoyant water to form a surface vortex (Linden 1991) introduces ageostrophic effects associated with the front where the edge of the buoyant vortex intersects the free surface. Here we investigate the flow produced by a source in the upper layer of a pre-existing two-layer rotating environment, thus removing these ageostrophic effects of the front. The water added at the source is of the same density as the water in the upper layer, and the consequent baroclinic vortex deforms the interface. However, the variations of layer depth are small compared with the layer depth, so that the flow is approximately quasi-geostrophic (QG). The second extension examines the behaviour of both anticyclonic and cyclonic vortices. A sink in the upper layer was used to generate baroclinic cyclonic vortices. In the geostrophic approximation there is no dynamical difference between cyclones and anticyclones of the same vorticity structure, and comparison between the source and sink experiments gives further information on the importance of ageostrophic effects in these flows.

The experimental apparatus is described in § 2. The results are given in § 3 and are compared with the one-layer results in § 4. The conclusions of the work are discussed in § 5.

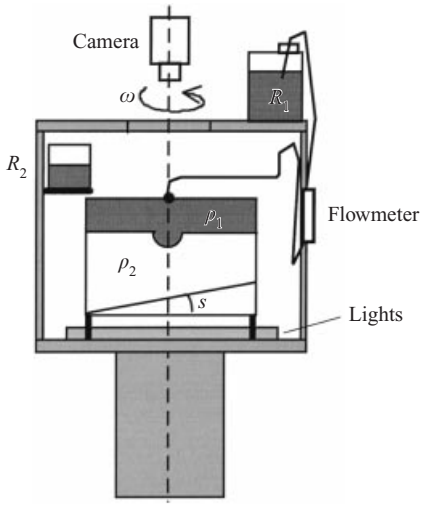

FIGURE 1. Diagram showing the experimental apparatus.

2. The experiments

A sketch of the apparatus is shown in figure 1. The experiments were conducted in a transparent Perspex tank of depth 35 cm with a square base measuring 45 cm. This was mounted on a direct-drive, 1m diameter, rotating turntable with a vertical axis of rotation. We used a square tank to avoid optical distortion from side views associated with a circular tank. The tank was centred on the vertical rotation axis of the table and had a bottom slope (s) to simulate the β-effect. The use of a sloping bottom to represent a β-plane is strictly valid only for a unstratified fluid. In the two-layer stratification used here, the slope provides an equivalent potential vorticity (PV) gradient in the lower layer, but there is not a direct representation of the PV gradient in the upper layer. Nevertheless, the thermal wind coupling across the interface implies that the motion in the upper layer is also influenced by the lower-layer PV gradient. Hence, the essential features of a β-plane are captured using a slope in this case where the shallowest part of the tank corresponded to the 'northern' shore of the northern hemisphere topographic β-plane. East was to the right looking onshore, west was to the left and south was the deepest end. A reservoir (R_1) of dyed fluid of density ρ_1 was connected to a flow meter through a plastic tube of 0.6 cm diameter. In turn the flow meter was connected through more plastic tube to a copper pipe, of 0.3 cm inner diameter, that ended in the middle of the tank. A small piece of sponge was attached to the open end of the pipe, so as to reduce the mixing between the flow from the pipe and the environment. A gravity-fed source was achieved by positioning the reservoir (R_1) on the top of the rotating table, and a sink was generated by fixing the reservoir (R_1) below the tank. In both cases the constant head driving the injection or withdrawal equates to a constant flow rate Q through the tube.

The two-layer environment was produced by first adding a layer of depth H_2 of water of density ρ_2 and leaving the whole system to come to a state of solid-body rotation. Dyed water, of density $\rho_1 < \rho_2$, was added from a reservoir (R_2) through a float at a low flow rate (in order to minimize mixing on the interface between the two layers) to form the second layer of depth H_1. The addition of the second layer caused a density interface perturbation, and the experiment was only started after this perturbation had decayed and the system was close to solid-body rotation.

Exp. no.	$f(s^{-1})$	$Q(cm^3\ s^{-1})$†	$g'(cm\ s^{-1})$	H_2/H_1	$W(cm)$‡
A	1.0	+3.0	0.36	0.32	15.9
B	3.3	+3.0	0.36	0.25	8.7
C	1.0	−2.0	0.46	0.33	12.6
D	3.3	−3.0	0.46	0.51	8.7

† $Q > 0$ for a source, $Q < 0$ for a sink.
‡ W is the north–south horizontal scale of the flow.

TABLE 1. Parameters in the experiments analysed with the particle tracking technique.

(Diffusion of the scalar, in this case salt, producing the density field means that complete solid-body rotation is not achieved. However, residual circulations were always a very small fraction ($\approx$1%) of the motions induced by the source or sink). For anticyclonic vortices, fluid of density ρ_1 from the reservoir R_1 was added at a constant flow rate Q through the source positioned at the surface of the second layer. For cyclonic vortices, fluid of density ρ_1 was withdrawn from the top layer into the reservoir R_1 at a constant flow rate Q through a pipe positioned at the surface of the upper layer. In both experiments the density difference was achieved by using salt solution as the lower layer. Consequently the two fluids were miscible and some mixing between them occurred along the interface of the two layers. However, the amount of mixing was small and is neglected (typically the interface was about 0.5 cm thick). The buoyancy forces were due to the reduced gravity $g' = g|\rho_2 - \rho_2|/\rho_2$, where g is the gravitational acceleration acting on the interface. In the experiments g' was fixed at $0.36\,cm\,s^{-2}$ except for Exp C and Exp D (see table 1) where $g' = 0.46\,cm\,s^{-2}$. The Coriolis parameter f varied from $0.6\,s^{-1}$ to $3.3\,s^{-1}$ and the slope of the bottom was fixed at $s = \tan\alpha = 0.42$, where α is the angle between the slope and the horizontal (see figure 1). The flow rate covered the range $0.55 \leqslant Q \leqslant 4.50\,cm^3\,s^{-1}$ and the ratio of the layer depths, measured in the middle of the tank, was fixed at $H_2/H_1 = 0.5$, except for the four experiments in table 1. The Rossby number of the vortices, defined as the absolute value of the ratio of the relative vorticity and the Coriolis parameter, ranged from 0.12 to 0.30 and the Rossby radius of deformation, $a = (g'H_1^{1/2}H_2^{1/2}f^{-2})^{0.5}$, varied from 0.57 cm to 3.15 cm.

Flow visualization and measurements of the velocity and depth fields were obtained from video recordings the flow. A video camera was mounted above the tank and fixed to the turntable so that the velocity measurements were obtained in the rotating frame. A mirror was set up on one side of the table in order to record a vertical side view of the vortices. The side view of the anticyclonic vortices (figure 2*a*) was visualized by dying the top layer and using the same dye concentration in the source fluid. For the cyclonic vortices (figure 2*b*) the bottom layer was dyed and clear water was drawn from the top layer through the sink.

In order to measure the depth fields for both anticyclonic and cyclonic vortices the top layer was dyed and the video camera recorded a plan view of the flow. The reduction in intensity of light transmitted through the top dyed layer during the experiment was measured and compared to that through the top dyed layer with no flow at the beginning of the experiment (for details see Cenedese & Dalziel 1998). In order to do this with the camera positioned above the tank light sources were placed under the tank. In fact this technique, also referred to as a measurement of optical thickness, gives a measure of the average concentration of the dye over

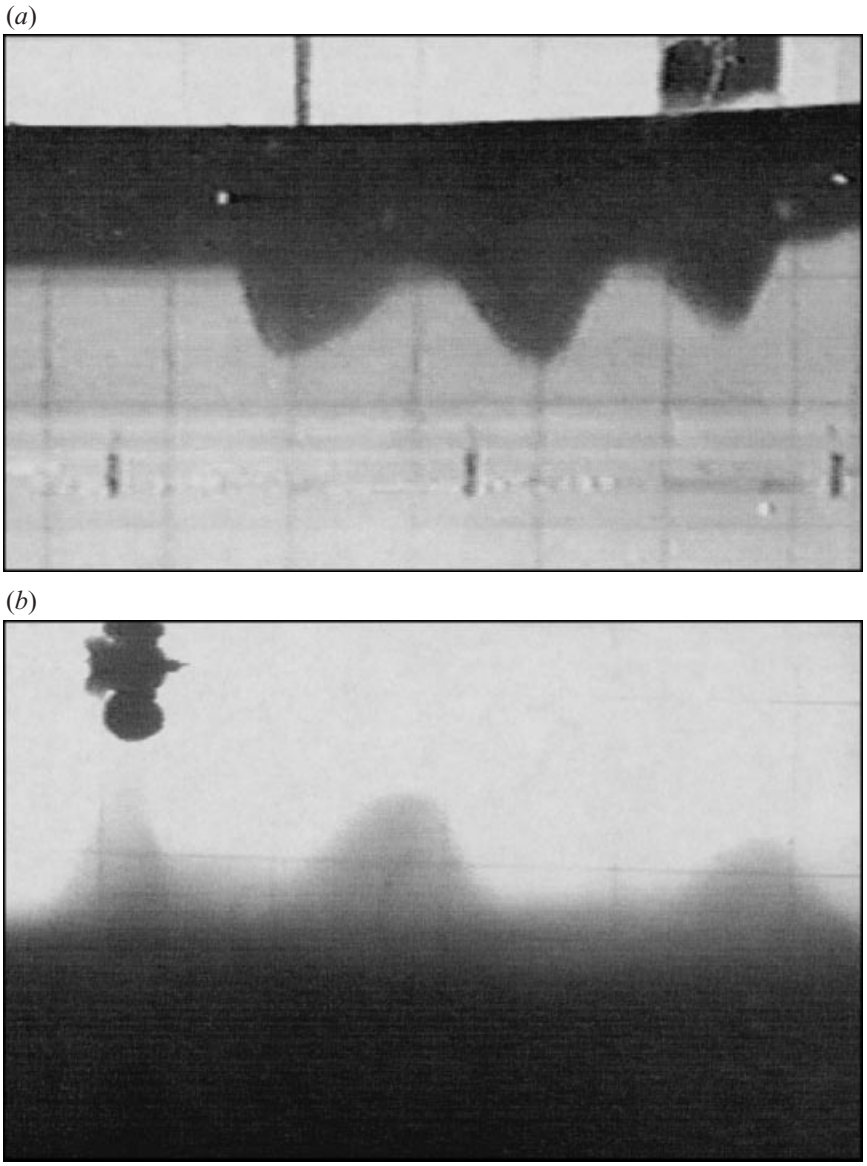

FIGURE 2. Side views of the density interface perturbation for multiple vortices generated by a source or a sink positioned at the left of the picture ($Q = 3.00\,\mathrm{cm\,s^{-1}}$, $f = 3.3\ \mathrm{s^{-1}}$). The vortices are propagating westward (to the right). The anticyclonic vortices (*a*) presented an almost parabolic shape downwards. The cyclonic vortices (*b*) had a density interface initially raised to a cusp by suction into the sink.

the whole fluid thickness H_1. However, since only one layer is dyed, with a uniform concentration of dye, the measure of the optical thickness gives the depth of the top dyed layer. The depth field of the lower layer was then obtained by subtracting the upper layer depth from the total depth of the fluid in the tank. We used a red food colour with a concentration 1 ml 1^{-1}. The software 'Diglmage' (Dalziel 1992) was used to determine intensity fields, to manipulate the recorded images and to find the intensity contours of the vortices in order to calculate their depths. The contours were

determined at time increments of Δt. For the single-vortex case the extreme western edge of the vortex, evaluated by sight, was located with an uncertainty < 0.6 cm. For the multiple-vortices case the position of the centre of each vortex was evaluated by sight with the same uncertainty. From these measurements the data were fitted by a straight line whose slope then gave the velocity U_i of the vortices, where $i = 1, 2, \ldots, n$, for n vortices in a run. When $i > 1$ the average velocity U was calculated.

A similar procedure was used to calculate the phase speed U_p of waves observed in the transition from single to multiple vortices described in § 3.1.1. In this case the intensity contour of the wave was marked and the position of the crest of the wave determined at set intervals of time.

The velocity fields inside the vortices were determined for four experiments with values of the parameters given in table 1. The velocity fields were obtained from video recordings of seeding particles placed in the flow. Pliolite VT particles, approximately 0.5 mm in diameter, were used as neutrally buoyant tracers of the flow. Pliolite VT is an opaque granular material used in the manufacture of paint. In may be ground and sieved to produce highly reflective particles of a desired size. The particles were located in the upper layer by a suitable choice of ρ_1 and ρ_2 and were illuminated at the interface between the two layers by a planar sheet of light from a slide projector. In all the experiments a horizontal light sheet 2 cm thick was used, and the velocities presented are the projections of the motion in this horizontal plane. The height of the light sheet was chosen so that the particles were observed outside the interfacial Ekman layers. At the low Rossby numbers of the vortices, the horizontal velocity is independent of depth, and so the measurements are representative of the field in each layer. The images obtained from the video records of the motion were digitized on a matrix 512×512 pixels with 8-bit precision. Therefore, each point of the field was represented by a light intensity value from 0 to 255. Illuminated particles were represented by high values of intensity. From this intensity information the centroid of each particle was determined and their trajectories were calculated by following the individual particles from one image to another. The velocity of each particle was calculated. Hence, the velocity field was transferred onto a 40×30 regular grid with $\Delta x = \Delta y = 1$ cm (figure 3 *a*) from which the vorticity field was determined (figure 3 *b*).

3. Results

3.1. *Regime regions*

3.1.1. *Anticyclonic vortices*

In the absence of friction the angular momentum of the source water was conserved and the fluid from the source rotated anticyclonically. At these rotation rates the velocity in each layer was independent of depth and an anticyclonic rotation was established beneath the source. The resulting shear across the interface caused a depression of the interface. Thus the anticyclonic vortex compressed columns of lower-layer fluid underneath it and, in accord with the conservation of PV, an anticyclonic motion was established in the lower layer as well. The lower-layer vortex continued to interact with the upper-layer vortex through advection of vorticity (Griffiths & Hopfinger 1986). The lower-layer vortex was influenced by the presence of a sloping bottom topography that induced a westward drift of the vortex. Consequently, the vorticity of the lower-layer vortex induced the drift of the upper-layer vortex at the same speed and any small departure from a configuration concentric with the

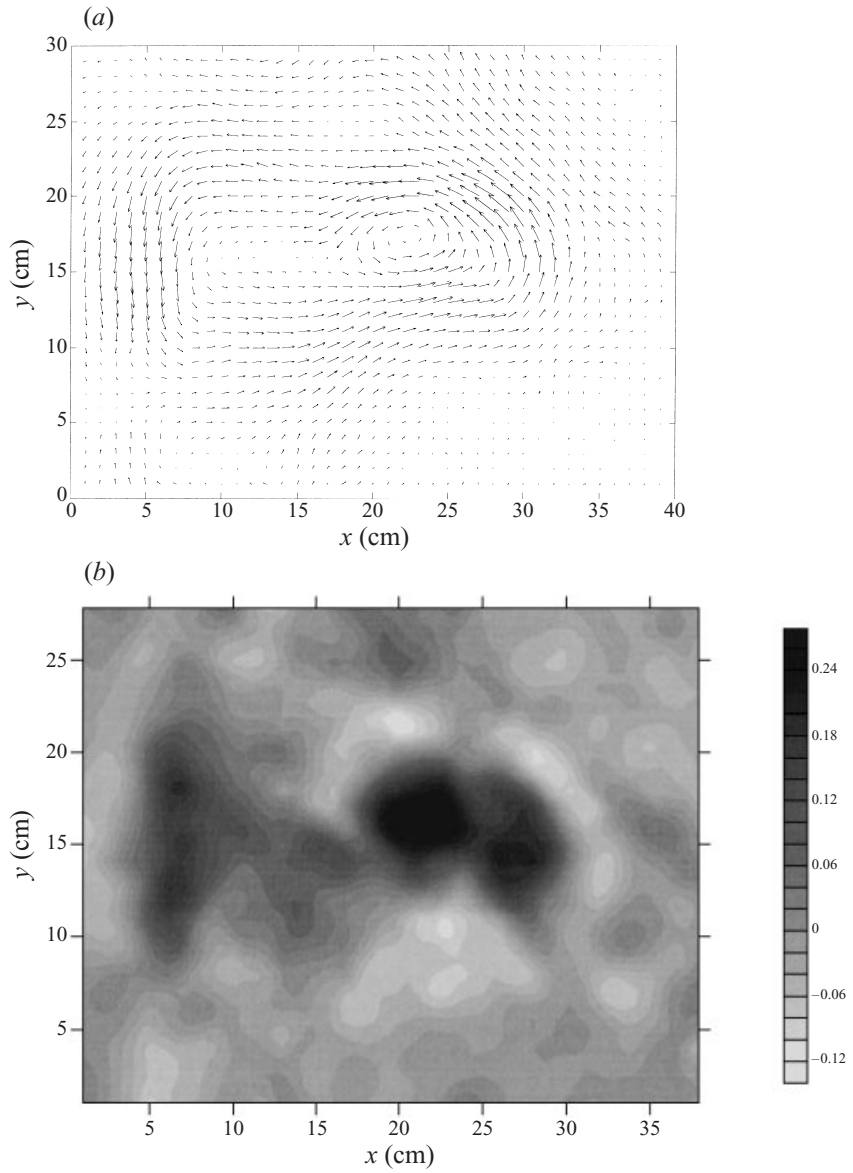

FIGURE 3. Exp. D after 17.3 rotation periods: (*a*) velocity field and (*b*) vorticity field. In these fields the reference system is as follows: right=east, left=west, top=north, bottom=south. The sink has the approximate coordinates (26,15) and the vortices are moving westwards.

lower-layer motion was removed by advection by the lower-layer velocity field. The Coriolis force was balanced by the pressure force due to the sloping density interface that was observed to dome downwards at the centre of the eddy and initially was almost parabolic (Griffiths & Linden 1981) as shown in figure 2(*a*). Three different forms of the response to the forcing were observed and these are described below.

Single vortex. For low values of the flow rate and of the Coriolis parameter a single vortex formed slightly to the south of the source. Initially the vortex adjusted to a cyclostrophic equilibrium state in which buoyancy, Coriolis and centrifugal forces

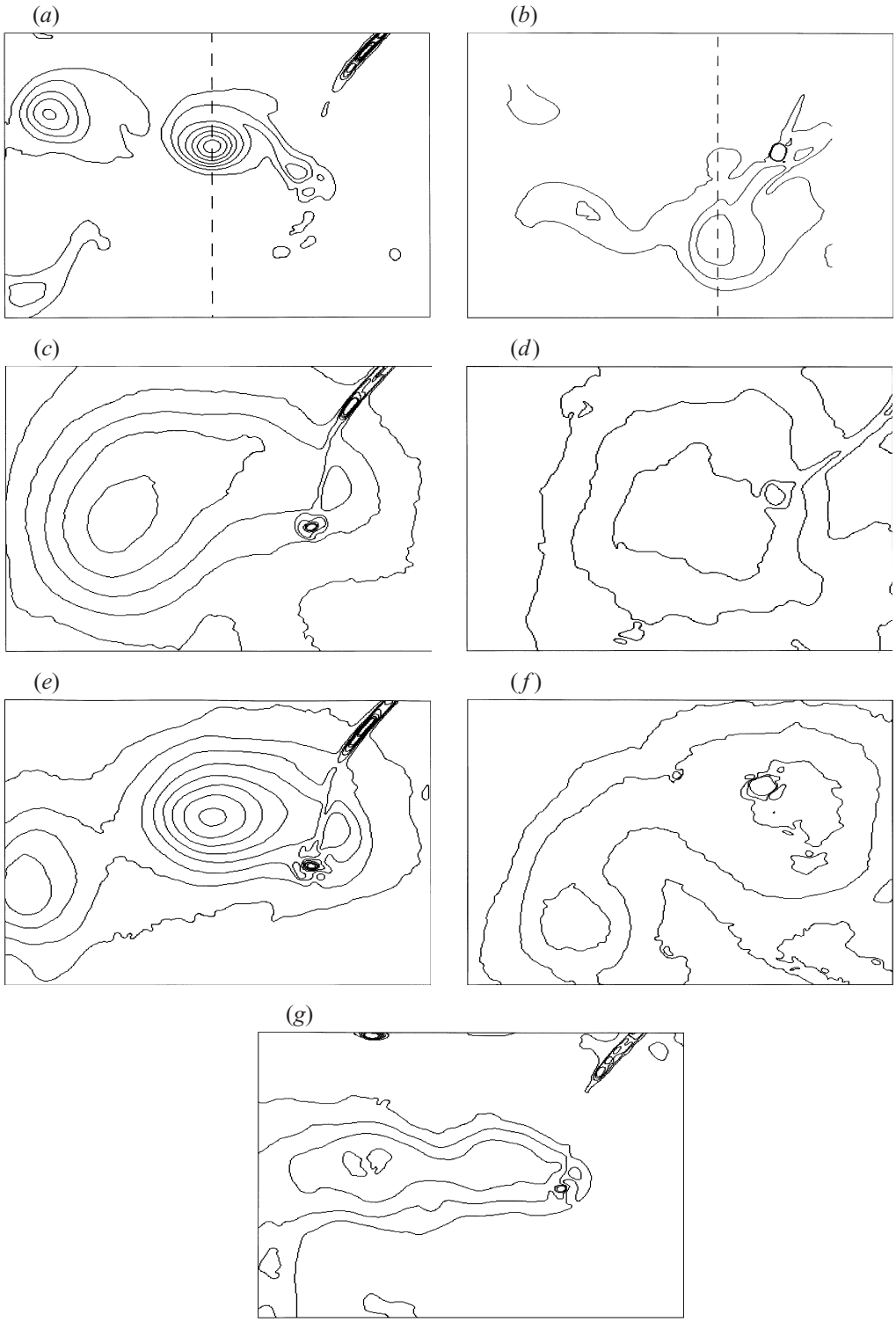

FIGURE 4. For caption see facing page.

are balanced, and presented an approximately axisymmetric shape. At later times the axisymmetric vortex was influenced by the presence of a sloping bottom and extended to the west as shown in figure 4 (*d*). Within the vortex the flow became nearly zonal (parallel to the isobaths), except near the source and at the leading edge of the vortex where there was a meridional motion (normal to the isobaths). The zonal flow was a consequence of the low Rossby number flow in the lower layer which follows the contours of constant depth. Where the motion was zonal, the circulation within the vortex was towards the west in the southern part and to the east in the northern part.

Multiple vortices. At larger values of the Coriolis parameter and the flow rate, a different behaviour was observed. A single vortex formed south of the source and then was observed to break free from the source and move to the west. It was then followed by a sequence of other vortices behaving in the same way, giving a chain of vortices extending to the west from the source (see figures 2 *a* and 4 *b*).

Transition from single to multiple. The transition from single to multiple vortices was investigated for low values of the Coriolis parameter and for all ranges of flow rates. A single vortex formed slightly south of the source and extended to the west (figure 5 *a*). Subsequently a perturbation moving westward was observed on the southern edge of the vortex as shown in figures 5 (*b*), 5 (*c*) and 5 (*d*) (looking at the lower-layer depth field represented by the grey scale). This perturbation acted on the single vortex in order to allow it to break free from the source as was observed in the multiple vortices regime. Some of these perturbations were able to detach fluid from the single bigger vortex (figures 4 *f* and 5 *c*). Subsequently this fluid formed a smaller anticyclonic vortex that moved towards the south west as an independent structure (figure 5 *d*). However, after this initial detachment, the single vortex continued to extend to the west and successive perturbations did not detach fluid from the single vortex. Instead, two vortices formed within the centre of the single vortex. Once the wave-like perturbation moved far to the west leaving the double vortex behind, the two vortices merged together again giving a single-vortex structure similar to that observed in the single regime. This process then repeated itself with more perturbations forming on the anticyclonic vortex and then travelling to the west. The time at which the first perturbation started developing varied between experiments and the time interval between these perturbations was not constant.

The flow regimes observed in experiments with different values of the flow rate Q and Coriolis parameter f, keeping g', H_1 and H_2 fixed, are summarized in figure 6 (*a*).

3.1.2. *Cyclonic vortices*

When upper-layer water was drawn at a constant flow rate from the top layer through a sink located at the free surface the water entering the sink rotated cyclonically around the sink in order to conserve its angular momentum. In an

FIGURE 4. Depth contour fields showing the cyclonic (a, c, e, g) and anticyclonic (b, d, f) regimes. (a, b) Multiple vortices after 24.7 rotation periods for $Q = 3.00\,\mathrm{cm\,s^{-1}}$, $f = 3.3\ \mathrm{s^{-1}}$. (c, d) Single vortex after 17.2 rotation periods for $Q = 3.00\,\mathrm{cm\,s^{-1}}$, $f = 0.60\ \mathrm{s^{-1}}$. ($e, f$) Transition regime (i) after 21.1 rotation periods for $Q = 3.00\,\mathrm{cm\,s^{-1}}$, $f = 0.80\,\mathrm{s^{-1}}$. ($g$) Transition regime (ii) after 81.7 rotation periods for $Q = 0.50\,\mathrm{cm\,s^{-1}}$, $f = 2.00\,\mathrm{s^{-1}}$. The sink/source is positioned on the right of the picture and the vortices are moving westward. The isobaths are represented by continuous lines and are drawn every cm.

https://doi.org/10.1017/S0022112098003644 Published online by Cambridge University Press

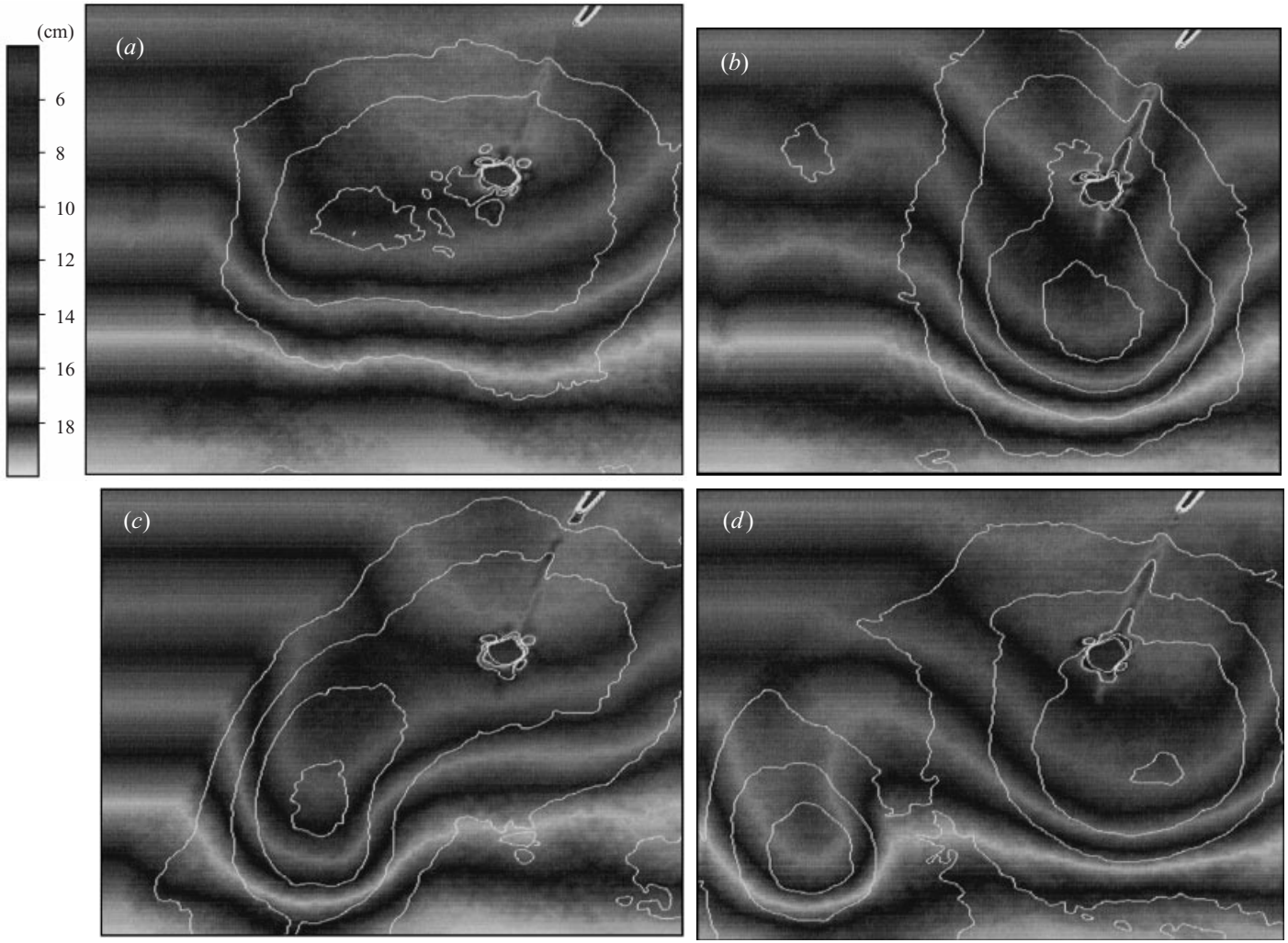

FIGURE 5. For caption see facing page.

analogous fashion to the anticyclonic vortices, cyclonic rotation was established throughout the top layer and the shear across the density interface lead to an upward doming of the interface beneath the vortex. This initially appeared as a cusp, as shown in figure 2(*b*). The doming of the interface stretches the lower-layer fluid underneath it and, as a result, a cyclonic motion is also established in the lower layer. There is a similar coupling across the interface of any non-axisymmetric motion in either layer through advection of vorticity as described in § 3.1.1, and a westward drift of the whole structure is induced by the sloping bottom. In this case four different forms of behaviour were observed as follows.

Single vortex. At small values of the Coriolis parameter a single vortex formed slightly to the north of the sink. After cyclostrophic adjustment the vortex was not symmetric but extended to the west (figure 4*c*) in a similar manner to the anticyclonic vortex described in § 3.1.1. Within the elongated vortex 'tube' the flow was nearly zonal, towards the east in the southern side and to the west in the northern side.

Multiple vortices. When the Coriolis parameter and the flow rate were increased a behaviour similar to that described in § 3.1.1. was observed. A single vortex formed in the centre of the tank north of the sink and was then observed to break free from the sink and move to the west followed by a sequence of essentially identical vortices (figures 2*b* and 4*a*). However, in these experiments the vortices were more coherent and axisymmetric than in the anticyclonic case.

Transition from single to multiple. The transition from single to multiple vortices was characterized by two different behaviours.

(i) A different structure developed for small values of the Coriolis parameter and for high flow rates (figure 4*e*). As in the multiple regime a single vortex formed north of the sink and extended to the west, later breaking free from the sink and moving west. Then a second single vortex developed but did not break free from the sink. This second vortex was not symmetric but extended to the west, as in the single regime, and within this vortex the flow was nearly zonal, except near the sink and at the leading edge of the vortex where there was a meridional motion.

(ii) For small values of the flow rate and for medium to large values of the Coriolis parameter a single vortex formed slightly north of the sink and extended to the west forming a tube-like structure with a zonal flow similar to that in the single regime. The single tube vortex then became distorted and acquired the structure of two more-circular vortices which were not completely separated from each other and with common circulation around their outer boundary, as shown in figure 4(*g*). These two vortices started moving to the west, as observed in the multiple vortex regime and, at a later stage, merged together to form a single vortex again. This re-formed single vortex had the same tube-like structure as at the beginning of the experiment and

FIGURE 5. Depth fields of the anticyclonic vortex in the transition regime for $Q = 3.00\,\mathrm{cm\,s^{-1}}$ and $f = 0.80\ \mathrm{s^{-1}}$. The isobaths of the lower layer are represented by grey levels shown in the legend, the isobaths of the interface perturbation are represented by continuous white lines and are shown for 1 cm depth intervals. The source is on the right of the picture. (*a*) The single vortex starts extending to the west (left) and (*b*) after 17.1 rotation periods a perturbation is visible on the southern edge of the vortex. (*c*) After 20.1 rotation periods the perturbation moves to the west and (*d*) removes some fluid from the single vortex after 22.17 rotation periods. A smaller anticyclonic vortex is then able to detach from the larger single vortex and to move towards the south-west as an independent structure.

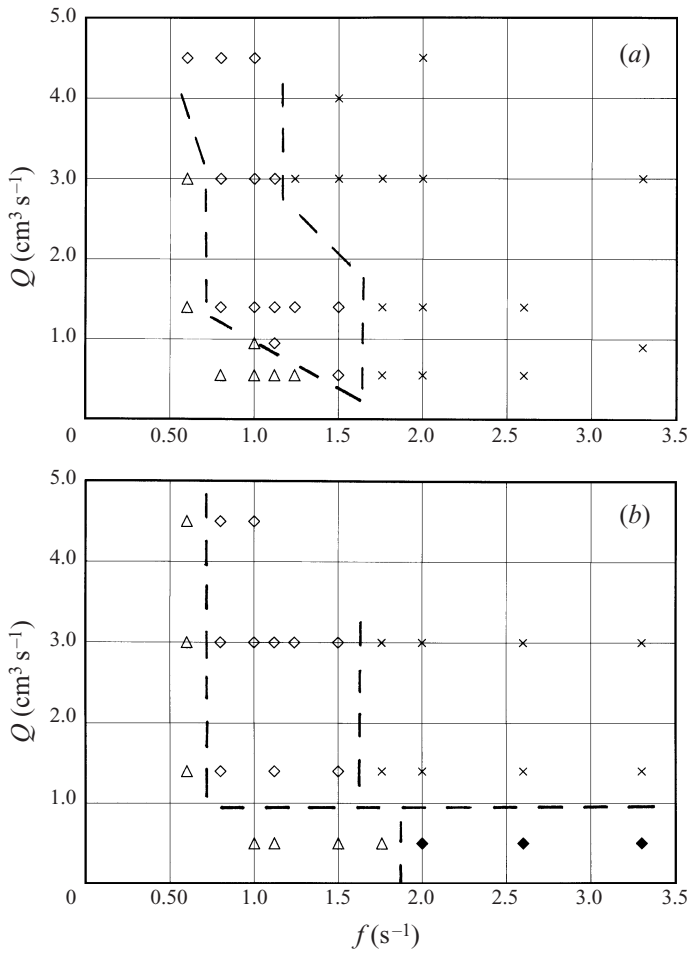

FIGURE 6. Regime diagram showing the transition from single to multiple anticyclonic (*a*) and cyclonic (*b*) vortices: ×, multiple vortices; △, a single vortex; ◇ vortices in transition zone (i); ◆, the vortices in transition zone (ii).

continued to extend to the west. The same behaviour occurred again at least once before the experiment was stopped.

The observed regimes are summarized in figure 6 (*b*) in terms of the flow rate and Coriolis parameter.

3.2. *Overall eddy properties*

3.2.1. *Westward velocity*

Measurements were made of the extreme western extent of the single vortex as defined by the position $x(t)$ (measured from the source $x = 0$) of the ± 0.5 cm depth contour. The results for two experiments, one with a source and the other with a sink, are shown in figure 7. For the cyclone the velocity is constant with distance, but for the anticyclone there is a deceleration when the westward front of the advancing vortex is about 12 cm from the source. This reduction in velocity was noticed in several experiments and may be due to an initially large speed caused by the divergent flow near the source. In general, the anticyclones were less coherent

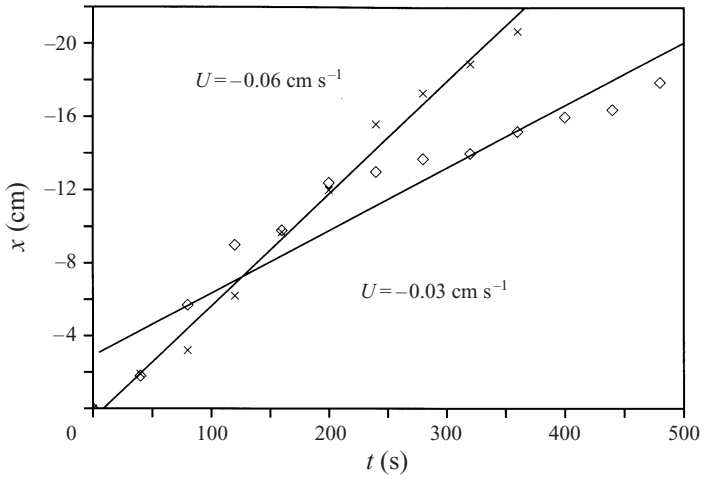

FIGURE 7. $x-t$ diagram for a single vortex. The slope of the lines (fit by least squares) represents the westward velocities U of the vortex. The $\diamond$ represent the anticyclonic vortex and the $\times$ the cyclonic vortex for $f = 0.6$ s^{-1} and $Q = 1.40$ cm^3 s^{-1}.

than the cyclones, possible due to ageostrophic effects, and their velocities showed more scatter. It should be noted that this deceleration does not appear to be due to the finite size of the tank which at the point of deceleration is a further 12 cm from the front. There is no evidence of blocking by the walls of the tank as cyclones or anticyclones approach the western boundary, and in all cases the sizes of the vortices, which scale with the Rossby deformation radius, are small compared to the size of the tank. A general result is that single cyclones travelled faster than the equivalent anticyclones.

Similarly, approximately constant velocities were observed for multiple vortices as shown in figures 8 (*a*) and 8 (*b*). Although there is some variation between the speed of the individual vortices, the differences are small and not systematic. There is no significant difference between the anticyclones and cyclones in this case. Figure 8 shows also the time scale for the vortex production (indicated by the offsets on the time axis), which was observed to vary between 10.8 and 15.7 rotation periods for cyclonic vortices and between 7.6 and 16.4 for the anticyclonic vortices. The vortices were shed at quite regular intervals and the time between successive vortices decreased as Q increased. The shedding frequency was practically independent of f over the range covered in these experiments.

The westward velocities increased linearly with either the flow rate or the Coriolis parameter when the other variable was fixed. The velocity U can be expressed as a function of the variables introduced in § 2:

$$U = \hat{F}(Q, f, s, g', H_1, H_2), \tag{1}$$

and by dimensional analysis the velocity is given by

$$U = \frac{Qf^2}{g'H_1} F\left(s, \frac{H_1}{H_2}, \frac{g'}{f^2 H_1}\right). \tag{2}$$

For fixed slope and ratio of layer depths and assuming F takes the form of a power

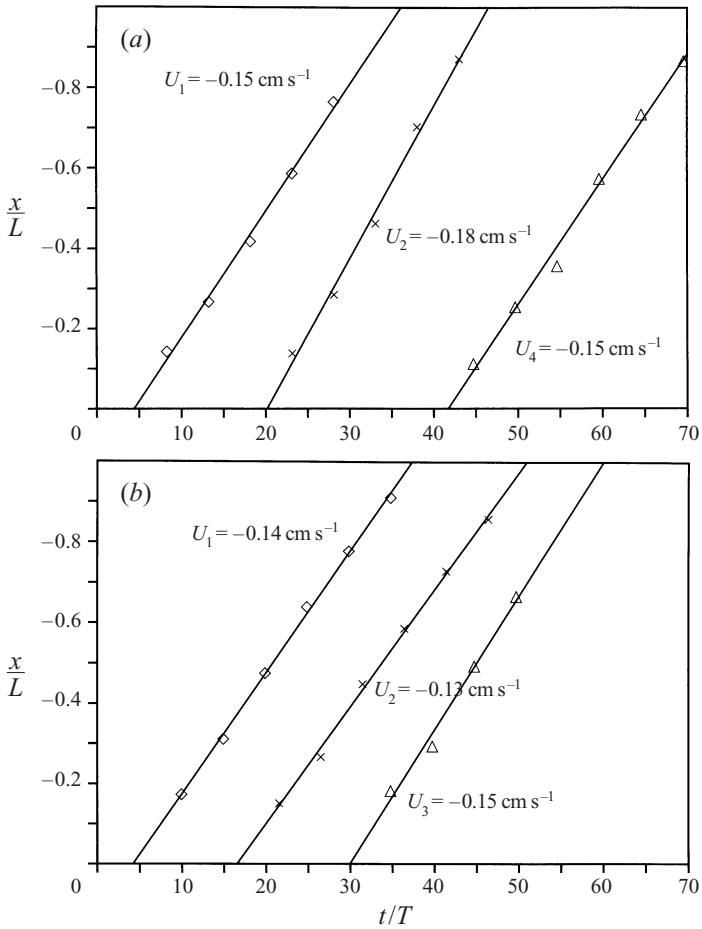

FIGURE 8. $x - t$ diagram for multiple anticyclonic (a) and cyclonic (b) vortices. The position x and the time t are non-dimensionalized using the tank half-width $L = 22.5$ cm and the rotation period $T = 4.8$ s, respectively. The slope of the fitting curves represents the westward velocities U_i of the multiple vortices for $f = 2.6$ s^{-1} and $Q = 1.40$ cm^3 s^{-1}. The $\diamond$ indicate the first, the $\times$ the second and the $\triangle$ the third vortex for the cyclones and the fourth vortex for the anticyclones. The time offset represents the time taken for a subsequent vortex to form.

law, the non-dimensional velocity can be expressed as

$$\frac{g' H_1 U}{Q f^2} = \alpha \left(\frac{g'}{f^2 H_1} \right)^{\gamma}, \tag{3}$$

$$\alpha = \alpha \left(s, \frac{H_1}{H_2} \right), \tag{4}$$

where α and γ are constants.

A simple scaling analysis may be obtained as follows. For the case of a single vortex, consider the flow rate Q given by

$$Q = c_s U W H_1, \tag{5}$$

where we assume c_s is a constant depending on the shape of the vortex, and the

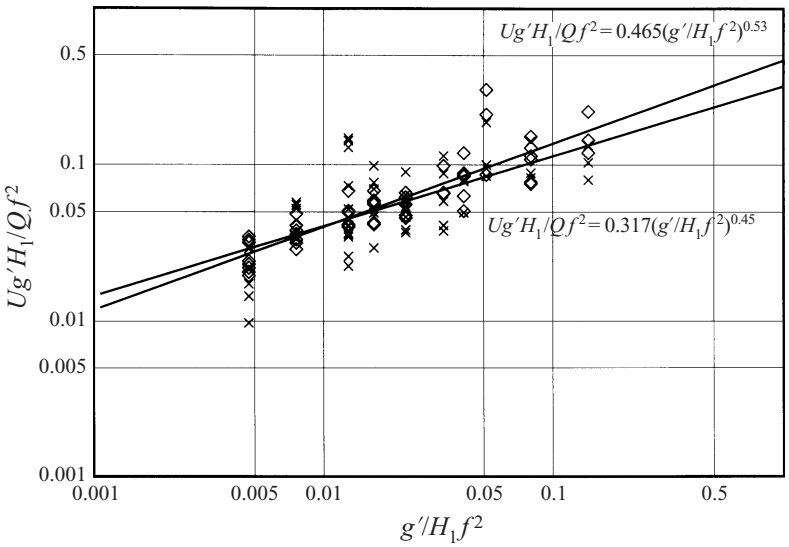

FIGURE 9. Non-dimensional westward velocities plotted against the non-dimensional parameter $g'f^{-2}H_1^{-1}$. For the cyclones ($\diamond$) the slope of the fitting curve is 0.53 and for the anticyclones ($\times$) it is 0.45. Data from both single and multiple vortices are included in this figure.

horizontal scale W in the north–south direction is given by the deformation scale

$$W^2 = c\frac{g'H_1}{f^2}, \tag{6}$$

where c is a constant. To be precise, H_1W should be replaced by the fluid volume of the upper layer moving with a westward velocity U. This volume depends on the shape and depth of the vortex and its determination is not trivial. We approximated this volume with H_1W knowing that this approximation is strictly valid only in the case of small interface perturbations.

Substituting (6) into (5) we obtain

$$U = c'\frac{Qf}{g'^{1/2}H_1^{3/2}}, \tag{7}$$

where $c' = 1/(c_s c^{1/2})$ is a constant and, dividing by $Qf^2/(g'H_1)$, (7) gives the non-dimensional velocity

$$\frac{g'H_1U}{Qf^2} = c'\left(\frac{g'}{f^2H_1}\right)^{1/2}. \tag{8}$$

For the case where multiple vortices form, different theoretical considerations have to be followed. Consider the time scale for the production of one vortex in this regime given by t_f. This is the time taken for the volume V of the eddy to be filled by buoyant fluid flowing at a flow rate Q. This time scale is also controlled by the time the vortex takes to move westward a distance equal to the diameter W of the vortex. If the eddy in the top layer is taken to have a cylindrical shape (within the approximation of small interface perturbations) its volume can be expressed as

$$V = \frac{1}{4}\pi c_s' W^2 H_1, \tag{9}$$

where c_s' is a constant depending on the shape of the vortex. Hence the flow rate is given by

$$Q = \frac{1}{4}\pi c_s' U W H_1. \tag{10}$$

Expression (10) is similar to (5) and the value of c_s and $\frac{1}{4}\pi c_s'$ are of the same order of magnitude. Therefore, even if different mechanisms are considered, the same expression (8) for the non-dimensional westward velocity is found for both single and multiple vortices.

The expressions found by dimensional analysis (3) and by scaling considerations (8) are equivalent providing $\gamma = 0.5$ and $c' = \alpha$. The measured value of the westward velocity of single vortices and of each of the multiple vortices non-dimensionalized as in (3) are plotted in figure 9 against the value of the non-dimensional parameter g'/f^2H_1. The figure shows the experimental values of γ equal to 0.45 and 0.53 for anticyclones and cyclones, respectively, which agree quite well with the theoretical value $\gamma = 0.5$. The value of the shape constants c_s and c_s' introduced in (5) and (9), respectively, are expected to be of order of unity and can be obtained from the experimental values of α. Assuming the constant $c = 4$ (i.e. the vortex radius is equal to the deformation scale), the experimental results in figure 9 give values of $c_s = 1.6$ and 1.1 for anticyclones and cyclones, respectively, and $c_s' = 2.0$ and 1.5. These results agree with the expected values for c_s and c_s' and support the theoretical scalings.

3.2.2. *Vortex morphology*

The study of the shape of the vortices highlighted important asymmetries between the anticyclonic and cyclonic vortices. A systematic difference in depth between cyclones and anticyclones was observed in every regime, with the cyclones being deeper. This difference was examined in detail by measuring the shape and morphology of both cyclones and anticyclones. The horizontal cross-sectional area and the volume are morphological characteristics highly dependent on the forcing. High flow rates increase both the area and volume, while high values of the Coriolis parameter decrease the Rossby radius of deformation and consequently the horizontal scale of the flow. In this section we will compare cyclonic and anticyclonic vortices generated by the same forcing, i.e. with the same values of the parameters f and Q, so that any difference observed will be associated with the different sign of vorticity or the effects of the source/sink.

From the depth fields (figures 4) the vortex edge was located by considering it to be represented by the depth contour ± 0.5 cm. This choice of contour is determined by the uncertainty in determining any depth contour ($< \pm 0.5$ cm), resulting mainly from noise and perturbations present in the flow environment before and during the experiments. In figure 4 the edge of the vortex is therefore represented by this outer depth contour. Both cyclonic and anticyclonic multiple vortices edges were fitted by an ellipse and the ellipticity, defined as the ratio of the meridional and the zonal axis, was measured in order to study and classify differences between vortices.

The main differences were noticed in the multiple regime so we will describe this regime first. The cyclones were quite elliptical in shape with the major axis oriented approximately east–west and a clear region of separation between each vortex was observed when looking at the depth field (figure 4*a*). The ellipticity of the vortices was approximately 0.6. The anticyclones presented a less regular shape with the major axis oriented more north–south and the ellipticity varied up to approximately 1.3. Furthermore the anticyclonic vortices were connected together at their outer

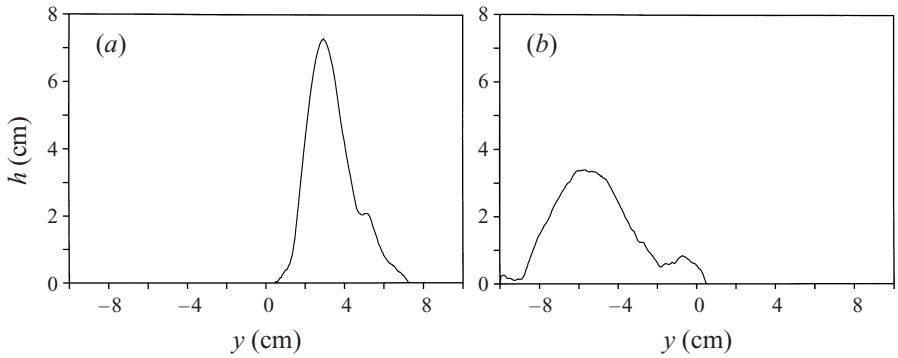

FIGURE 10. North–south depth sections for multiple cyclones (*a*) and anticyclones (inverted) (*b*) along the dashed lines in figures 4(*a*) and 4(*b*), respectively. The cyclones were observed to be deeper and less spread out than the anticyclones.

boundary, as shown in figure 4(*b*), giving a less compact and coherent structure than the cyclones. The size of the vortices, measured in the north–south direction, decreased with increasing Coriolis parameter and, in keeping with the scaling analysis, was observed to be approximately equal to the Rossby radius of deformation. For cyclones, the size increased from 5.3 cm to 14.4 cm from the multiple to the single regime while the anticyclone size increased from 10.1 cm to 14.6 cm.

The other major difference between cyclones and anticyclones is their vertical profile. Figure 10 shows an example of this difference; the cyclone is deeper and narrower than the anticyclone. This is a general result. The volumes of the vortices produced at the same Q and f, on the other hand, are very similar. Those shown in figures 4(*a*) and 4(*b*), respectively, were calculated by integrating the depth fields and gave values of 98 cm^3 for the cyclone and 103 cm^3 for the anticyclone. It is interesting to note that for these vortices the volume obtained by multiplying the source/sink flow rate and time between successive vortices gave values of 144 cm^3 and 130 cm^3 for the cyclone and anticyclone, respectively. These values are comparable with, but larger than, the volume of the vortices and are consistent with the scaling arguments given in § 3.2.

Similar qualitative differences in the orientation and the shape of the vortex were observed in the single-vortex regime. Again the cyclonic vortex was deeper and narrower than the anticyclone for the same external parameters. In both regimes the major difference in the shape is associated with the interface profile rather than horizontal area at the level of the interface. While cyclones present a somewhat smaller surface area (sometimes as small as one-half the size of the equivalent anticyclone) at the level of the interface, the major difference is in the depth. In fact, cyclones are well represented by cones while anticyclones are better represented by paraboloids. For the vortices shown in figure 10, a conical fit for the cyclone gives a maximum depth of 6.9 cm compared with the observed maximum of 7.2 cm, and a paraboloidal fit to the anticyclone gives a maximum depth of 3.6 cm compared to the observed value 3.4 cm.

The importance of this difference in interface profile results from the fact that at low Rossby number, the thermal wind balance holds and so the azimuthal velocity shear across the interface is different in the two cases, and in general larger for the cyclones. The reasons for the difference are not entirely clear but we suspect they are due to nonlinear behaviour associated with flow close to the source/sink. This point is discussed further in § 5.

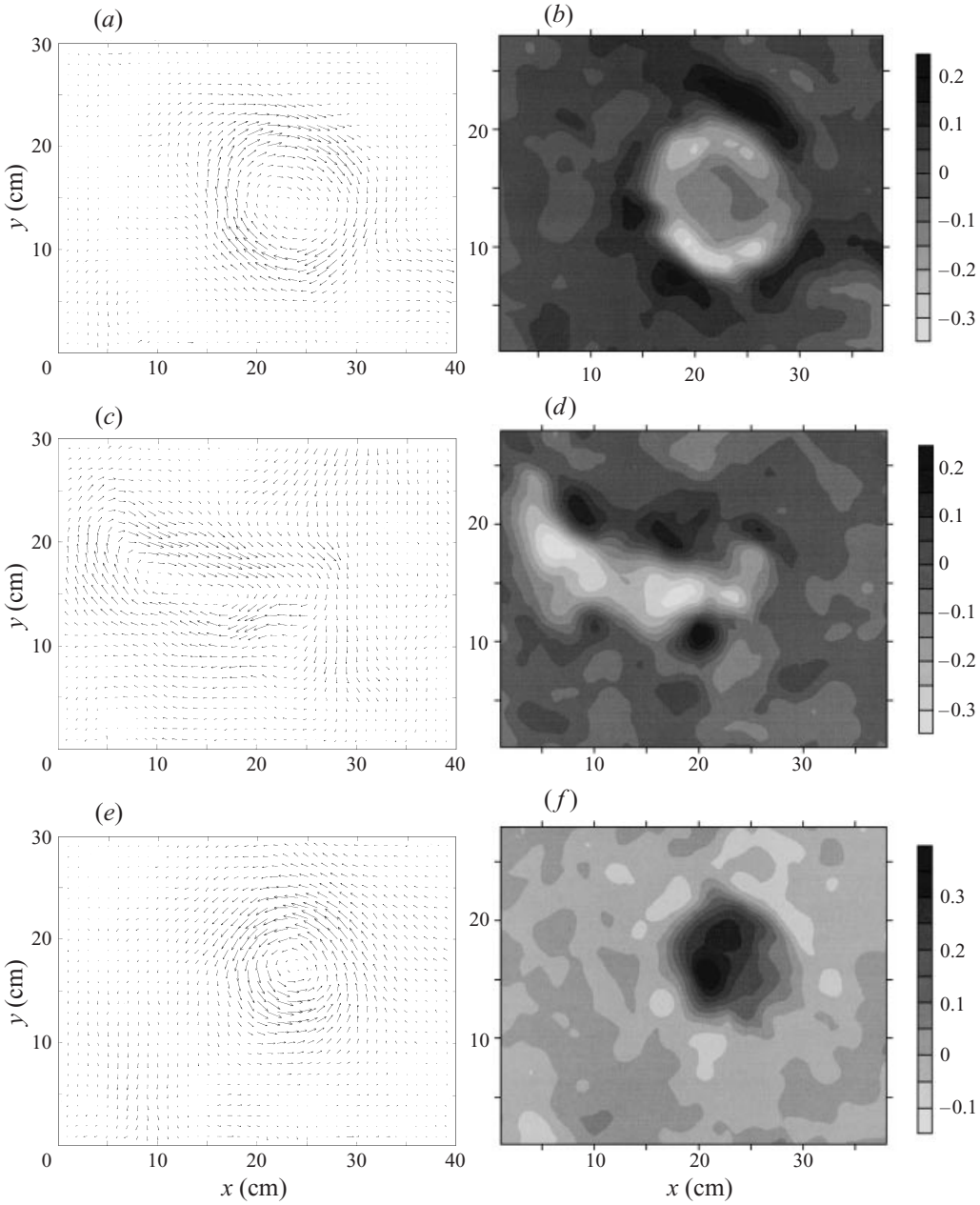

FIGURE 11. Velocity (*a*, *c*, *e*) and vorticity (*b*, *d*, *f*) fields. (*a*, *b*) Exp. A anticyclones after 13.4 rotation periods; (*c*, *d*) exp. B anticyclones after 36.7 rotation periods; (*e*, *f*) exp. C cyclones after 13.4 rotation periods. In these fields the reference system is as follows: right=east, left=west, top=north, bottom=south. The source (or sink) has the approximate coordinates (26,15) and the vortices are moving westwards.

3.3. *Velocity and vorticity fields*

From the velocity fields calculated for the four experiments given in table 1, the vorticity fields were derived as shown in figures 11 and 12. The single anticyclonic vortex in Exp. A is shown in figure 11 (*a*, *b*) for a time before the development of the

wave-like structure. The vorticity field shows a non-uniform anticyclonic vorticity in the interior, with the strongest vorticity associated with streaming motion near the edge (associated with the interface slope – see figure 10), and at the edge of the vortex there are smaller patches of cyclonic vorticity. The maximum relative vorticity ζ was $0.30\,\mathrm{s}^{-1}$ and the Rossby number Ro of the vortex, defined as the absolute value of the ratio of the relative vorticity and the Coriolis parameter, was 0.25. The anticyclonic multiple state was observed during Exp. B (figure 11 *c*, *d*) and the two light grey regions in the vorticity field represent the two vortices moving westward. In this case the maximum anticyclonic vorticity occurred at the centre of each vortex. Weak cyclonic vorticity is also present along the boundary of the vortices. In this regime the maximum value of the vorticity was $\zeta = 0.30\,\mathrm{s}^{-1}$ and $Ro = 0.09$. Figure 11(*e*,*f*) shows the characteristic cyclonic motion that develops in the transition regime (i) (described in § 3.1.2). Here the vorticity is maximum at the centre and decreases outwards. The maximum vorticity $\zeta = 0.35\,\mathrm{s}^{-1}$ gives a Rossby number 0.30.

A detailed development of the cyclonic multiple vortices is given in figure 12. A single vortex was observed after 8.1 rotation periods. After 22.0 rotation periods and 35.7 rotation periods the second vortex and the third vortex developed respectively and are illustrated in figure 12 (*d*, *h*). The vortex positioned at the left-hand side of the figure developed from a residual background motion present at the beginning of the experiment. As already observed for the anticyclonic vortices, weak vorticity of opposite sign is present along the edges of the cyclonic vortices. In this experiment a strong anticyclonic vortex also developed at the left end of the vortex chain. In this regime the maximum vorticity was $\zeta = 0.35\,\mathrm{s}^{-1}$, giving $Ro = 0.10$.

We also calculated the ratio between the maximal orbital velocity in the field and the westward velocity of the vortex. For single and multiple vortices the anticyclones had a ratio of 4.5 and 2.0, respectively. For single and multiple cyclones similar values of 6.0 and 1.5 respectively, were obtained. These results showed that the azimuthal velocity within the vortices was larger than their westward velocities, particularly for the single vortices. The shape of the vortices was harder to define from the vorticity fields (figures 11 and 12) than from the depth fields (figure 4). In the vorticity fields shown in figures 11 (*b*) and 11 (*f*), the vortices after 13.4 rotation periods had just started departing from the axisymmetric shape acquired during geostrophic adjustment. The multiple vortices shown in figures 11 (*d*) and 12 are approximately elliptical but with no preferential orientation, in contrast to that observed in the depth fields discussed in § 3.2. The difference is due to the fact that the vorticity fields are less accurate than the depth fields. However, the horizontal scale in the north–south direction was measured from the vorticity field and the results, shown in table 1, are similar to the horizontal scales determined from the depth fields as reported in § 3.2.

4. Comparison with one-ambient-layer case

The flow generated by a source of buoyant fluid in a two-layer environment was observed to behave in a qualitatively similar way to that formed by injecting buoyant water at the surface of a single layer (Linden 1991), where there are ageostrophic effects associated with the front where the vortices intersect the free surface. The linear theory for a steady flow in a one-ambient-layer system (Linden 1991) shows that non-zero velocities are found only in the forced region or directly west of it and no meridional motion occurs outside the forced region. In addition, if the scale of the forced region is $O(1)$ then the surface perturbation is $O(q/U_s)$ where q is the volume flux per unit area of the source and U_s is the linear topographic Rossby wave

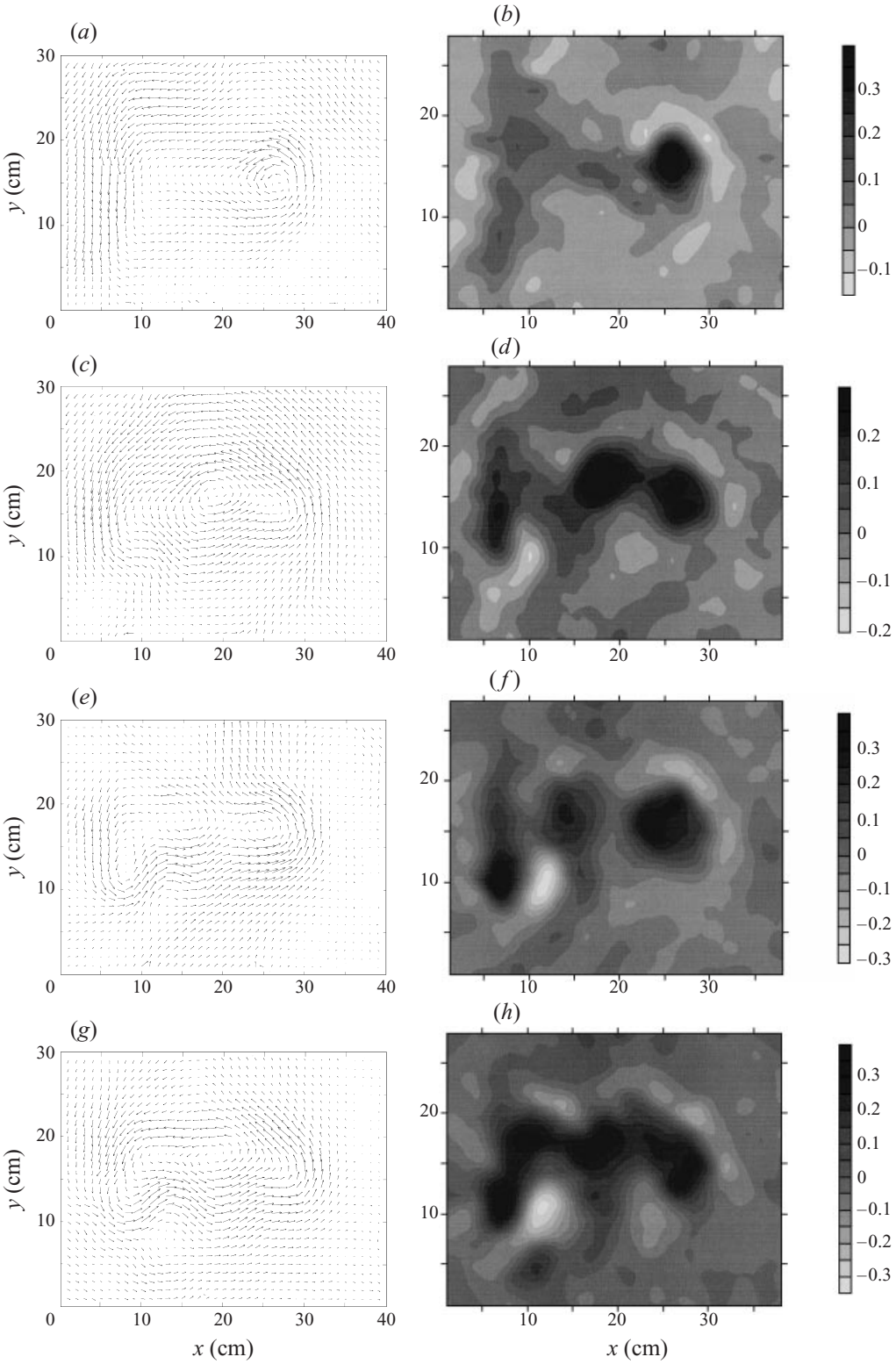

FIGURE 12. For caption see facing page.

speed. Hence the linear theory requires $q \ll U_s$. The linear flow is stable provided the northward gradient of the potential vorticity does not change sign (Linden 1991). This criterion is satisfied for

$$q \leqslant s\frac{sg'}{f} = sU_s, \tag{11}$$

where s is the slope of the bottom. If we take the westward velocity U of the vortex as a measure of q, (11) becomes

$$U \leqslant sU_s. \tag{12}$$

This stability criterion is an application of Rayleigh's inflection point theorem, which is only valid for quasi-geostrophic flow. The experimental results from the one-ambient-layer case only partially agree with (12), as shown in figure 13. The intensity of the forcing (flow rate and the Coriolis parameter) determined the type of behaviour of anticyclonic vortices in a two-ambient-layers system as well and the experimental results gave a better agreement with (12) as shown in figure 13. This difference, along with a different behaviour in the transition regime, indicates that the ageostrophic effects associated with the front may play a role in the transition from single to multiple anticyclonic vortices.

In the anticyclonic transition regime described in § 3.1.1 the westward velocity of the single vortex did not satisfy (12) as strictly as in the single-vortex region and some vortices had a velocity $U > sU_s$ (figure 14). The wave-like perturbation observed in this regime was travelling westward with a phase velocity U_p greater than the linear topographic Rossby wave speed U_s, as shown in figure 14, and therefore was not linear.

The stability criterion (12) was also applied to the cyclonic vortices. The westward velocities of the vortices in the single and multiple regimes satisfied (12) with the exception of one single vortex that had a velocity U slightly larger than sU_s (figure 15). In the cyclonic transition regime (ii) we measured the westward velocities of both the single and the double vortices but they did not show any relation with (12).

5. Discussion and conclusions

A source or a sink of buoyant fluid in a two-layer rotating environment with a sloping bottom generates *baroclinic* anticyclonic or cyclonic vortices. Strong ageostrophic effects associated with a bounding density front are avoided. The comparison between the two-ambient-layers and the one-ambient-layer cases shows that the ageostrophic effects associated with the front may play a role in the processes associated with the transition from single to multiple anticyclonic vortices. The difference lies in the flow behaviour in the transition regime and in the westward propagation speeds. However, the qualitative behaviour was essentially the same. For low flow rates a single vortex formed at the source and extended to the west. At higher flow rates the vortex broke free from the source and moved to the west, followed by a chain of vortices behaving similarly. The results suggest that QG theory gives a reasonable indication of the stability of the flow in the one-ambient-layer case, but nevertheless there remain ageostrophic effects associated with the front-like behaviour at the edge

FIGURE 12. Exp. D velocity (*a*, *c*, *e*, *g*) and vorticity (*b*, *d*, *f*, *h*) fields after (*a*, *b*) 8.1, (*c*, *d*) 22.0, (*e*, *f*) 27.3, and (*g*, *h*) 35.7 rotation periods. In these fields the reference system and the sink are positioned as in figure 11. The vortices, represented by the darkest regions in the vorticity field, are moving westward.

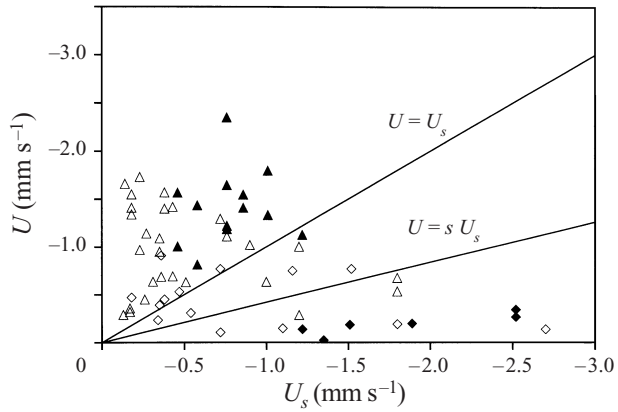

FIGURE 13. Westward velocity U vs. U_s for single (◆) and multiple (▲) anticyclonic vortices in a two-ambient-layer system, and for single (⋄) and multiple (△) vortices in a one-ambient-layer system (Linden 1991).

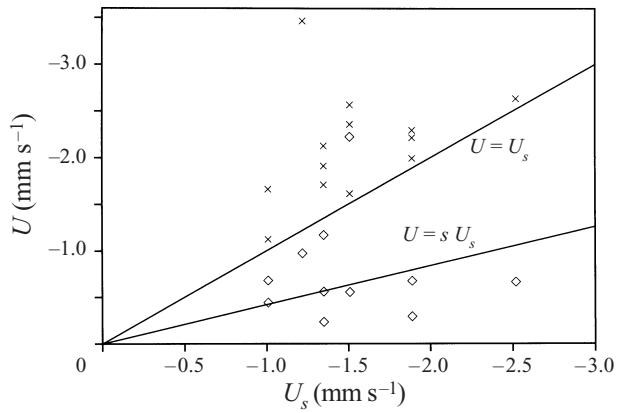

FIGURE 14. Westward velocity U_p for the wave-like perturbation (×), and the single vortex U(⋄), observed in the anticyclonic transition regime (as defined in § 3.1.1).

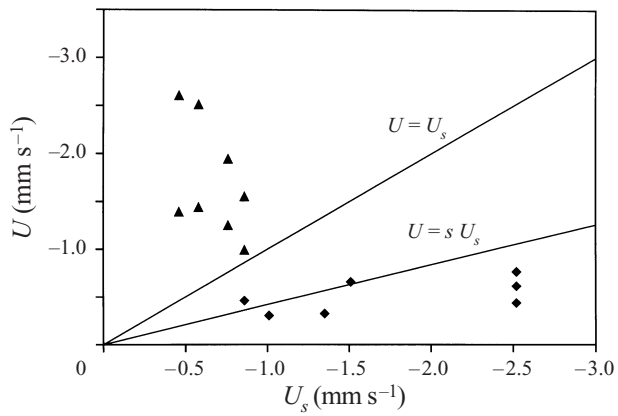

FIGURE 15. Westward velocity U vs. U_s for single (◆) and multiple (▲) cyclonic vortices.

of the vortex. Similar conclusions were drawn by Holford (1994) who examined the baroclinic instability of an isolated vortex on an f-plane in one-layer environment.

The flow produced by a sink allowed us to investigate the behaviour of baroclinic cyclones in the two-layer environment. For both the case of a source and of a sink, the vortices adjusted to a QG balance which is a cyclostrophic equilibrium in which buoyancy, Coriolis and centrifugal forces are balanced. The presence of the centrifugal term is associated with the curvature of the vortex. In both cases the ratio of the magnitude of the centrifugal force to the Coriolis force is equal to the Rossby number, which for the vortices described here was $Ro \leqslant 0.3$. The sign of the centrifugal force is opposite to the sign of the Coriolis force in the case of cyclones and anticyclones, and so this may account for some of the differences in their observed behaviour. This adjustment took place to the north of the sink for cyclones, whereas it was to the south of the source for anticyclones. This difference can be explained by considering the advection of fluid columns upslope and downslope: the so-called beta gyre. A cyclonic vortex advects fluid columns downslope on the western side of the vortex, and upslope on the eastern side. The opposite is true for an anticyclonic vortex. Conservation of PV dictates that the columns advected upslope and downslope acquire anticyclonic and cyclonic relative vorticity, respectively. These regions of positive and negative vorticity form a dipolar contribution to the velocity field which can then induce motion across the slope. This motion is northward for cyclones and southward for anticyclones. After the QG adjustment the vortices drifted westward due again to the presence of the sloping bottom. This drift can be explained with the same mechanism described above. Both cyclonic and anticyclonic vortices advect fluid columns upslope toward the north side of the vortex, and downslope toward the south side. Conservation of PV now leads to a dipolar relative vorticity distribution that induces a westward motion along the slope. The Rossby numbers for the flows are small but finite (< 0.3) and hence the motions are only expected to be approximately QG. By definition, QG motion must be exactly the same for cyclones and anticyclones if the vorticity distributions are the same; however, the shape of the interface perturbation generated by the two different type of vortices appeared to be substantially different (figure 10) and also the shape and the orientation of the vortex depended on the sign of the vorticity field. A systematic difference in the depth field between cyclones and anticyclones was observed in every regime region, the cyclones being deeper for the same external parameters. This difference was examined by looking in detail at the shape and morphology of both cyclones and anticyclones. The forcing mechanism producing anticyclones and cyclones generates a radial divergent and convergent flow, respectively, localized underneath the forcing region. In addition, the anticyclones are produced by the injection of low-PV fluid, while for the cyclones the fluid withdrawn has the PV of the upper layer. In both cases there is some modification of the PV as a result of interfacial Ekman layers. The differences in the characteristics of the radial divergent and convergent flow, and therefore the asymmetry in the forcing mechanism, could be responsible for the asymmetry between anticyclones and cyclones. This asymmetry was observed in the quantitative properties of the vortices and also during the qualitative transition from the single to the multiple regime. However, cyclones and anticyclones showed the same qualitative behaviour in both the single and multiple regimes despite the obvious differences associated with the radial convergent and divergent flow.

The application of the stability criterion (12) involves the determination of the westward velocity of the vortices. By dimensional analysis we found a scaling for this velocity and it was confirmed by comparison with the experimental results. The

translation velocities were also observed to be smaller than the azimuthal velocities within the vortices, especially in the single regime.

The transition from single to multiple vortex regimes occurred at greater values of Q and f for cyclones than for anticyclones (figure 6) and exhibited asymmetries so that different patterns of behaviour for anticyclones and cyclones were observed. This difference implied that some ageostrophic effects were still present in the flow. In addition, the occurrence of perturbations travelling westward with phase speed U_p greater than the linear topographic Rossby wave speed U_s (figure 14) is evidence that nonlinear effects were important in the flow. Such perturbations were not formed for cyclones, for which a smaller vortex broke away from the main vortex (transition regime (i) in figure 4). In this regime measured westward velocities did not give a coherent picture and it is difficult to explain the observed behaviour. A new behaviour was observed in the cyclonic transition regime (ii), where the westward velocities revealed that the single vortex was moving faster than the double vortex. Our interpretation is that the single vortex was travelling too quickly to remain single and so split in two separate vortices. In turn, the two vortices were travelling too slowly to remain separate and so merged together to give a single vortex again. However, in these experiments there was no correlation between the measured westward velocities and the linear topographic Rossby wave speed U_s. In this regime the behaviour of the two multiple vortices merging together to give a single vortex might also be related to the mechanism discussed by Griffiths & Hopfinger (1987). The stability boundary for coalescing of baroclinic vortices on a f-plane, shown in figure 10 of Griffiths & Hopfinger (1987), indicates that the conditions under which vortices combine depend on the Rossby radius of deformation. For the experiment showed in figure 4(*g*) the value of the relevant parameters λ/R' and d/R' are 0.28 and 2.6, respectively, where λ is the internal Rossby radius, R' is the vortex core radius and d is the distance between two vortices. These values would lead to coalescence for zero bottom slope. However, in our experiments there is uncertainty in the value of R'. Furthermore, λ/R' is close to 0.2, where baroclinic instability occurs because the horizontal lengthscale of the flow is large compared with the Rossby radius (Griffiths & Linden 1981). Although the criterion is only approximate, it indicates that there may be a competition in the transition regime (ii) between the coalescing of vortices having small Rossby radii or large core sizes, and splitting of the vortex so produced. The transition regimes show characteristics of both the multiple and single regimes, highlighting how a perturbation could move the flow towards the multiple regime whereas dissipation of this perturbation could restore the single regime.

For horizontal scales much larger than the Rossby radius of deformation ($B \ll 1$), asymmetry between anticyclones and cyclones has been found in numerical calculations derived from the shallow-water equation by Matsuura & Yamagata (1982). They suggested that this is due to nonlinearities in the geopotential surface associated with eddies. In their model this difference in the surface structure appears to make the anticyclones more coherent and stable structures. In our experiments the multiple anticyclones were generated by smaller values of the forcing but were observed to be less coherent than the multiple cyclones. Other types of experiments performed in a parabolic vessel show that, for the same values of the parameters, both cyclones and anticyclones are formed, but that the latter are significantly more robust (Nezlin & Sutyrin 1994).

One purpose of this study was to investigate some of the basic physical processes operating in the Canary Basin where Mediterranean water is found in lens-shaped vortices (Meddies). The results of laboratory experiments described in this paper

sugggest that a constant source of high flow rate of fluid can generate discrete vortices. Therefore, Meddies could be generated by a similar mechanism when the Mediterranean outflow through the Strait of Gibraltar has a sufficiently large flow rate. Typical values for the Mediterranean outflow upstream of Cape St. Vincent are $g' \approx 10^{-3}\,\mathrm{m\,s^{-2}}$, $f \approx 10^{-4}\ \mathrm{s^{-1}}$ and $s \approx 0.06$, where s includes both the effect of the β-plane and the effect of the bottom topography. These correspond to a linear topographic Rossby wave speed $U_s \approx 60\,\mathrm{cm\,s^{-1}}$. The observed drift speeds of Meddies are $5\,\mathrm{cm\,s^{-1}}$, which are small compared with U_s but are comparable with sU_s. These experiments suggest therefore, that it may be possible for the continuous outflow to break into isolated structures. The ocean, though, is further complicated by wind stress, complex topography and tide-controlled flow rates, all of which may influence the flow and affect the comparison with the laboratory experiments.

Partial support for C. C. was provided by a TMR fellowship, MAS3-CT96-5017.

REFERENCES

Armi, L., Hebert, D., Oakey, N., Price, J., Richardson, P. L., Rossby, T. & Ruddick, B. 1988 The history and decay of a Mediterranean salt lens. *Nature* **333**, 649–651.

Armi, L. & Zenk, W. 1984 Large lenses of highly saline Mediterranean water. *J. Phys. Oceanogr.* **14**, 1560–1576.

Bower, A. S., Armi, L. & Ambar, I. 1997 Lagrangian observation of Meddy formation during a Mediterranean undercurrent seeding experiment. *J. Phys. Oceanogr.* **27**, 2545–2575.

Cenedese, C. & Dalziel, S. B. 1998 Concentration and depth fields determined by the light transmitted through a dyed solution. *Exp. Fluids.* (Submitted).

Davey, M. K. & Killworth, P. D. 1989 Flow produced by discrete sources of buoyancy. *J. Phys. Oceanogr.* **19**, 1279–1290.

Dalziel, S. B. 1992 *DigImage: System Overview*. Cambridge Environmental Research Consultants, Ltd. 43 pp.

Griffiths, R. W. & Hopfinger, E. J. 1986 Experiments with baroclinic vortex pairs in a rotating fluid. *J. Fluid Mech.* **173**, 501–518.

Griffiths, R. W. & Hopfinger, E. J. 1987 Coalescing of geostrophic vortices. *J. Fluid Mech.* **178**, 73–97.

Griffiths, R. W. & Linden, P. F. 1981 The stability of vortices in a rotating, stratified fluid. *J. Fluid Mech.* **105**, 283–316.

Holford, J. M. 1994 The evolution of a front. PhD thesis, DAMTP, Cambridge University.

Linden, P. F. 1991 Dynamics of Fronts and Eddies. *Proc. Enrico Fermi Summer School*, pp. 313–351.

Matsuura, T. & Yamagata, T. 1982 On the evolution of nonlinear planetary eddies larger than the radius of deformation. *J. Phys. Oceanogr.* **12**, 440–456.

Nezlin, M. V. & Sutyrin, G. C. 1994 Problems of simulation of large, long-lived vortices in the atmospheres of the giant planets (Jupiter, Saturn, Neptune). *Surveys in Geophys.* **15**, 63–99.

Pingree, R. D. & Le Cann, B. 1993 Structure of a meddy (Bobby 92) Southeast of the Azores. *Deep-Sea Res.* **40**, 2077–2103.